geosciences

MDPI

Article

Analytical Modelling of Contaminant Transport in One-Dimensional Porous Medium Domains: The Fourier-FFT Approach

Rafid al Khoury * and Cor Kasbergen

Faculty of Civil Engineering and Geosciences, Delft University of Technology, Mekelweg 5, 2628 CD Delft, The Netherlands; c.kasbergen@tudelft.nl
* Correspondence: r.i.n.alkhoury@tudelft.nl

Abstract

Analytical solutions for contaminant transport in porous media are important for understanding subsurface processes and validating numerical models. However, conventional Laplace-transform-based approaches often face difficulties in handling realistic transient boundary conditions and typically result in challenging inverse formulations that require computationally intensive convolved integration. To address these limitations, this paper presents a Fourier-FFT analytical framework for solving the well-established one-dimensional advection–dispersion–reaction (ADR) equation in homogeneous and heterogeneous porous domains. The proposed Fourier-FFT approach enables straightforward mathematical formulation, rapid computation, and incorporation of realistic transient boundary conditions beyond idealized step or impulse inputs. Verification against a Laplace-based analytical solution for a homogeneous domain and a finite element solution for a dual-permeability domain show good agreement, confirming the accuracy of the method. Parametric analyses further demonstrate that the framework captures the expected physical behaviour of contaminant transport under varying hydrogeological and reaction conditions.

Keywords: contaminant transport; ADR; porous media; subsurface environment; analytical model; Fourier method; fast Fourier transform (FFT); dual-permeability domain

1. Introduction

The contaminant transport in ground subsurface is a topic of significant environmental and public health interest. Subsurface contamination often arises from industrial activities, agricultural runoff, and improper waste disposal, leading to the infiltration of hazardous substances into soil and aquifers. Once infiltrated, these contaminants can migrate through the porous media of the subsurface environment, potentially reaching drinking water sources, agricultural fields, and aquatic ecosystems. The resulting exposure can have serious consequences for human health and can cause harmful impacts on flora and fauna. Accurately understanding and predicting the behaviour of contaminants in subsurface environments is, therefore, essential for effective risk assessment, environmental protection, and remediation planning. This important topic has been widely covered in literature, including works) covered in literature [1–5].

Mathematical modelling of contaminant transport typically involves solving partial differential equations (PDEs) that represent key chemo-bio-physical processes such as

Academic Editor: Maurizio Barbieri

Received: 3 April 2026
Revised: 19 May 2026
Accepted: 24 May 2026
Published: 29 May 2026

advection, diffusion, and chemical reactions. Numerical methods offer versatility in handling nonlinear reaction processes, and complex geometries and boundary conditions, making them widely applicable for real-world scenarios, see [6–8], among others. However, developing and implementing these models can be technically demanding and often requires specialized expertise and powerful computational tools. In this context, analytical methods remain highly valuable, particularly during the initial stages of investigation or when validating numerical results. They offer simplified solutions that require minimal computational resources and expertise, while also enhancing conceptual understanding.

Many one-dimensional and multi-dimensional analytical models have been introduced in literature. Most current analytical models for contaminant transport rely on the Laplace transform or Green's function techniques, including works covered in literature [9–12]. Notable one-dimensional analytical models, which constitute the focus of this paper, include those proposed by van Genuchten and Alves [13], van Genuchten [14,15], Leij et al. [16], van Genuchten et al. [17,18], and Park and Zhan [19].

While the Laplace transform is a powerful tool for solving partial differential equations, its inverse often leads to complex semi-infinite integrals involving convolved transcendental functions. Even for the simplest form of the advection–dispersion (AD) equation (without production or decay), the classic work of Ogata and Banks [20] clearly demonstrates the extent of the mathematical complexity involved in deriving an analytical solution through Laplace inversion. Although numerical inversion techniques can be employed to evaluate these integrals, they are often computationally demanding and may suffer from stability and convergence limitations for highly transient or strongly coupled systems. Furthermore, Laplace transform–based solutions are usually limited to idealized inputs such as Dirac delta or step functions, which are rarely representative of real-world boundary conditions for contaminant transport problems.

Several studies have previously employed Fourier and spectral methods for solving transport problems in porous media. In many cases, these approaches were developed for fractional advection–dispersion equations describing anomalous or non-Fickian transport processes, where Fourier transforms provide an efficient means for handling fractional derivatives in spectral space [21,22]. Other studies utilized spectral or collocation discretization techniques, in which the solution is approximated using orthogonal basis expansions such as Fourier modes or Chebyshev polynomials [23,24].

Analytical Fourier-transform approaches for the classical advection–dispersion equation remain comparatively limited in the contaminant transport literature. For example, Bai et al. [25] employed Laplace transform in the time domain and Fourier integral transforms in the spatial domain to derive analytical transport solutions in porous media. Most existing Fourier-based formulations employ spectral transforms in the spatial domain or focus primarily on numerical spectral discretization methods. In contrast, the present study applies the Fourier transform in the time domain and combines it with the fast Fourier transform (FFT/IFFT) implementation to develop a systematic analytical framework for solving linear advection–dispersion–reaction boundary value problems with arbitrarily time-varying boundary conditions. This distinction enables straightforward treatment of random or measured temporal input signals while avoiding the mathematically cumbersome inverse-transform procedures commonly associated with classical Laplace-transform approaches. For further details on the spectral representation of boundary value problems, see Doyle [26] and Al Khoury and Kasbergen [27].

In this study, the Fourier-FFT approach is utilized to solve contaminant transport in homogeneous and fractured one-dimensional porous media. Various physical processes, including adsorption, decay, and production reactions, together with a range of boundary conditions, are addressed.

2. One-Dimensional Contaminant Transport in Homogeneous Porous Domains

The contaminant transport equation provides a mathematical framework for describing and predicting the movement of pollutants through porous media. For a one-dimensional homogeneous domain, it is expressed as

$$\underbrace{R\frac{\partial c}{\partial t}}_{\text{accumulation}} + \underbrace{v\frac{\partial c}{\partial x}}_{\text{advection}} = \underbrace{D\frac{\partial^2 c}{\partial x^2}}_{\text{hyd. dispersion}} + \underbrace{\mu c}_{\substack{\text{first-order}\\ \text{decay rate}}} + \underbrace{\dot{m}}_{\substack{\text{zero-order}\\ \text{production rate}}} \tag{1}$$

where $c\,(x,t)$ (kg m^{-3}) represents the species concentration, D (m^{2}s^{-1}) is the hydrodynamic dispersion coefficient, v (ms^{-1}) is the fluid velocity, $\dot{m}$ (kg m^{-3}s^{-1}) is production rate with zero-order, and μ (s^{-1}) represents a first-order reaction or decay constant. R in Equation (1) represents adsorption, defined as

$$R = 1 + \rho K_d/\varphi \tag{2}$$

in which ρ (kg m^{-3}) denotes the bulk density of the porous medium, K_d (m^{3}kg^{-1}) is the distribution coefficient (also referred to as the partition coefficient), and φ is the porosity. In the case of no adsorption, $R = 1$.

This equation is often referred to as the one-dimensional Advection–Dispersion–Reaction (ADR) equation. It accounts for processes such as advection (the bulk movement of fluid), diffusion (molecular movement of contaminants), and dispersion (the spreading of contaminants due to velocity variations within pores). Solving this equation offers insights into the behaviour of contaminants, including their spread, reactions, and interactions with the surrounding medium. Such insights are vital for evaluating potential risks and developing effective strategies for pollution mitigation and remediation.

In this paper, we present analytical solutions for contaminant transport problems occurring in both finite and infinite one-dimensional domains. We focus on solving the ADR equation with varying complexity.

2.1. Contaminant Transport with No Production or Decay

Contaminant transport without production or decay describes the movement of a chemical species through a medium where it is neither generated nor consumed. In such cases, the species' concentration remains unchanged during transport, with no additional sources or sinks influencing its amount in the domain. Mathematically, it corresponds to the Advection–Dispersion–Reaction (ADR) Equation (1), without the production and reaction terms on the right-hand side. To explore this scenario, we solve the equation under various geometries and boundary conditions to examine how different factors influence contaminant transport within the porous medium.

2.1.1. Semi-Infinite 1D Domain with Dirichlet Boundary Condition

In this scenario, we consider the transport of a contaminant within a semi-infinite one-dimensional domain, where the concentration is specified at the boundary (Dirichlet condition), as depicted in Figure 1. The boundary value problem for this case is given by

$$D\frac{\partial^2 c}{\partial x^2} - v\frac{\partial c}{\partial x} - R\frac{\partial c}{\partial t} = 0$$
$$\begin{aligned} \text{IC}: \quad & c(x,0) = 0 \\ \text{BC}: \quad & c(0,t) = C_0(t) \\ & c(\infty,t) = 0 \end{aligned} \tag{3}$$

in which $C_0(t)$ (kgm^{-3}) is some species concentration at boundary $x = 0$ that may be constant or a function of time.

Figure 1. Semi-infinite domain.

Applying the Fourier transform to Equation (3) yields

$$\frac{d^2\hat{c}}{dx^2} - \frac{v}{D}\frac{d\hat{c}}{dx} - \frac{i\omega}{\alpha}\hat{c} = 0$$
$$\begin{aligned} \text{BC}: \quad & \hat{c}(0,\omega) = \hat{C}_0(\omega) \\ & \hat{c}(\infty,\omega) = 0 \end{aligned} \tag{4}$$

in which $\alpha = D/R$ (m^{2}s^{-1}). Note that, the Fourier transform is usually abbreviated as

$$c(x,t) = \sum_n \hat{c}_n e^{i\omega_n t}, \text{ or } c(x,t) \Leftrightarrow \hat{c}(x,\omega_n), \text{ or } c(x,t) \Leftrightarrow \hat{c}_n \tag{5}$$

where the symbol $\Leftrightarrow$ indicates "transformed into" and is valid in both directions, and the hat in $(\hat{c})$ denotes that the variable has been transformed [26]. Note that while the analytical derivation is formulated in the continuous frequency domain using ω, the numerical implementation discretizes the spectrum into a finite set of frequencies ω_n, enabling efficient computation through the FFT/IFFT algorithm.

Transient (time-dependent) boundary value problems are typically expressed in terms of space and time derivatives. The Fourier representation, also denoted as spectral representation, of the time derivative of Equation (3) is

$$\frac{\partial c(x,t)}{\partial t} = \frac{\partial}{\partial t}\sum_n \hat{c}(x,\omega_n) e^{i\omega_n t} = \sum_n i\,\omega_n \hat{c}(x,\omega_n) e^{i\omega_n t} \tag{6}$$

This identity is usually abbreviated as

$$\frac{\partial c}{\partial t} \Rightarrow i\omega_n \hat{c}_n \text{ or } i\omega\hat{c} \tag{7}$$

This spectral representation clearly indicates that the time derivative of the state variable has been replaced by an algebraic expression, reducing thus the number of derivatives in the governing differential equation.

Similarly, the Fourier representation of the spatial derivative of Equation (3) is

$$\frac{\partial c(x,t)}{\partial x} = \frac{\partial}{\partial x}\sum_n \hat{c}(x,\omega_n) e^{i\omega_n t} = \sum_n \frac{\partial \hat{c}(x,\omega_n)}{\partial x} e^{i\omega_n t} \tag{8}$$

In shorthand notation, this identity can be expressed as

$$\frac{\partial c}{\partial x} \Rightarrow \frac{\partial \hat{c}_n}{\partial x}, \text{ or } \frac{\partial \hat{c}}{\partial x} \tag{9}$$

where in this case there is no reduction in the order of the derivative because the transformation used in this example is specifically designed to convert the time domain into the frequency domain.

For higher order derivatives, the temporal and spatial derivatives are represented by

$$\begin{array}{l} \frac{\partial^m c}{\partial t^m} \Rightarrow i^m \omega_n^m \hat{c}_n, \text{ or } i^m \omega^m \hat{c} \\ \frac{\partial^m c}{\partial x^m} \Rightarrow \frac{\partial^m \hat{c}_n}{\partial x^m}, \quad \text{or } \frac{\partial^m \hat{c}}{\partial x^m} \end{array} \tag{10}$$

As the coefficients in Equation (4) are constant, the trial solution can be $\hat{c} = ae^{\kappa x}$, in which a and κ are both constants that need to be determined. Substituting this trial solution into Equation (4) produces two eigenvalues that lead the general solution to become

$$\begin{array}{l} \hat{c} = a_1 e^{\kappa_1 x} + a_2 e^{\kappa_2 x} \\ \text{with} \\ \kappa_1 = \frac{1}{2D}\left(v - \sqrt{v^2 + 4\frac{i\omega}{\alpha}D^2}\right),\ \kappa_2 = \frac{1}{2D}\left(v + \sqrt{v^2 + 4\frac{i\omega}{\alpha}D^2}\right) \end{array} \tag{11}$$

Since the real part of κ_2 in this equation always yields positive values, the second boundary condition necessitates that $a_2 = 0$ in Equation (11), otherwise the solution becomes unbounded at far distances. Thus, the solution reduces to

$$\hat{c} = a_1 e^{\kappa_1 x} \tag{12}$$

At $x = 0$, the first boundary condition implies $a_1 = \hat{C}_0$ and hence, for a given frequency ω_n, the solution of Equation (4) yields

$$\hat{c}\,(x, \omega_n) = \hat{C}_0\, e^{\kappa_1 x} \tag{13}$$

Having obtained the solution in the frequency domain, the contaminant distribution in the time domain can then be calculated using the inverse fast Fourier transform (IFFT) algorithm, such that

$$c\,(x,t) = \sum_n \hat{c}\,(x, \omega_n)\, e^{i\omega_n t} \tag{14}$$

2.1.2. Finite 1D Domain with a Dirichlet–Neumann Boundary Condition

In this scenario, we examine the transport of a contaminant in a finite one-dimensional domain, with a specified concentration at one boundary (Dirichlet condition) and a zero-flux condition at the other boundary (Neumann condition), as shown in Figure 2. This configuration is commonly used to model situations where the contaminant enters a closed or confined domain at a controlled concentration while ensuring no net flow across the opposite boundary.

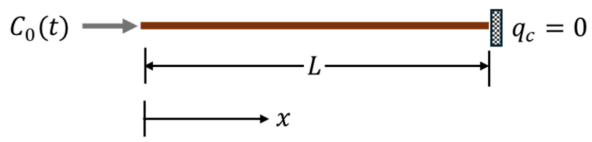

Figure 2. Finite domain.

The boundary value problem of a contaminant transport for this scenario can be expressed as

$$D\frac{\partial^2 c}{\partial x^2} - v\frac{\partial c}{\partial x} - R\frac{\partial c}{\partial t} = 0$$

$$\begin{aligned} \text{IC}: \quad & c(x,0) = 0 \\ \text{BC}: \quad & c(0,t) = C_0(t) \\ & \left.\frac{\partial c(x,t)}{\partial x}\right|_{x=L} = 0 \end{aligned} \tag{15}$$

where L is the length of the domain.

Applying the Fourier transform to Equation (15) gives

$$\frac{d^2\hat{c}}{dx^2} - \frac{v}{D}\frac{d\hat{c}}{dx} - \frac{i\omega}{\alpha}\hat{c} = 0$$

$$\begin{aligned} \text{BC}: \quad & \hat{c}(0,\omega) = \hat{C}_0(\omega) \\ & \left.\frac{d\hat{c}(x,\omega)}{dx}\right|_{x=L} = 0 \end{aligned} \tag{16}$$

As illustrated in the previous case, the general solution of the differential equation in Equation (16) is

$$\begin{aligned} & \hat{c} = a_1 e^{\kappa_1 x} + a_2 e^{\kappa_2 x} \\ & \text{with} \\ & \kappa_1 = \tfrac{1}{2D}\left(v - \sqrt{v^2 + 4\tfrac{i\omega}{\alpha}D^2}\right),\ \kappa_2 = \tfrac{1}{2D}\left(v + \sqrt{v^2 + 4\tfrac{i\omega}{\alpha}D^2}\right) \end{aligned} \tag{17}$$

Solving Equation (17) for the boundary conditions at $x = 0$ and $x = L$ and substituting into Equation (17) yields the solution of this boundary value problem for a given frequency ω_n, such that

$$\hat{c}(x,\omega_n) = \frac{\hat{C}_0}{1 - \frac{\kappa_1}{\kappa_2}e^{(\kappa_1-\kappa_2)L}}e^{\kappa_1 x} + \frac{\hat{C}_0}{1 - \frac{\kappa_2}{\kappa_1}e^{(\kappa_2-\kappa_1)L}}e^{\kappa_2 x} \tag{18}$$

Having solved the problem in the frequency domain, the solution in the time domain can then be obtained using the inverse fast Fourier transform (IFFT) algorithm, such that

$$c(x,t) = \sum_n \hat{c}(x,\omega_n)\, e^{i\omega_n t} \tag{19}$$

2.1.3. Finite 1D Domain with Robin–Neumann Boundary Conditions

This case investigates contaminant transport in a finite one-dimensional domain, where a Robin condition is applied at one boundary and a Neumann (zero-flux) condition at the other, as sketched in Figure 3. The Robin boundary condition models scenarios involving partial flux or exchange with the environment, such as absorption or chemical reactions, while the Neumann boundary ensures no net flux across the opposite boundary. This setup is particularly relevant for studying transport processes in confined systems with boundary interactions, enabling a detailed analysis of how such conditions influence contaminant behaviour and distribution.

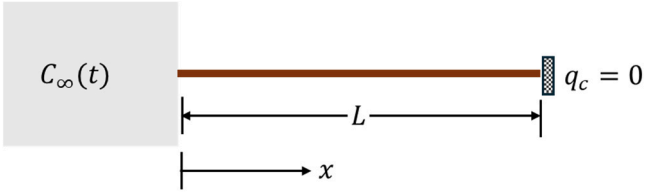

Figure 3. Finite domain surrounded by a polluted environment.

The boundary value problem of a pollutant transport for such a scenario is given by

$$\begin{aligned} & D\frac{\partial^2 c}{\partial x^2} - v\frac{\partial c}{\partial x} - R\frac{\partial c}{\partial t} = 0 \\ & \text{IC}: \quad c\,(x,0) = 0 \\ & \text{BC}: \quad \left(-D\frac{\partial c}{\partial x} + vc\right)\Big|_{x=0} = vC_\infty(t) \\ & \qquad \frac{\partial c}{\partial x}\Big|_{x=L} = 0 \end{aligned} \tag{20}$$

in which C_∞ (kgm^{-3}) is a contamination source at $x = 0$.

As explained above, the general solution of the differential equation in Equation (20) is

$$\begin{aligned} & \hat{c} = a_1 e^{\kappa_1 x} + a_2 e^{\kappa_2 x} \\ & \text{with} \\ & \kappa_1 = \tfrac{1}{2D}\left(v - \sqrt{v^2 + 4\tfrac{i\omega}{\alpha}D^2}\right),\ \kappa_2 = \tfrac{1}{2D}\left(v + \sqrt{v^2 + 4\tfrac{i\omega}{\alpha}D^2}\right) \end{aligned} \tag{21}$$

Applying the boundary conditions at $x = 0$ and $x = L$, solving the resulting equations simultaneously and then substituting into Equation (21), the solution of this boundary value problem for a given frequency ω_n results in

$$\begin{aligned} \hat{c}\,(x,\omega_n) = \ & \frac{\kappa_2 v\hat{C}_\infty}{(-D\kappa_1+v)\,\kappa_2 - (-D\kappa_2+v)\,\kappa_1 e^{(\kappa_1-\kappa_2)L}} e^{\kappa_1 x} + \\ & \frac{-\kappa_1 v\hat{C}_\infty}{(-D\kappa_1+v)\,\kappa_2 e^{(\kappa_2-\kappa_1)L} - (-D\kappa_2+v)\,\kappa_1} e^{\kappa_2 x} \end{aligned} \tag{22}$$

Using the IFFT algorithm, the solution of the boundary value problem given in Equation (20) in the time domain can then be obtained via

$$c\,(x,t) = \sum_n \hat{c}\,(x,\omega_n)\, e^{i\omega_n t} \tag{23}$$

2.2. Mass Transport with Zero-Order Production

Mass transport with zero-order production describes the movement of a chemical species through a medium while being generated at a constant rate. In this context, the transport process is governed by mechanisms such as advection and dispersion, with the addition of a production rate influencing the distribution of the species. Mathematically, it corresponds to solving the advection–dispersion–reaction (ADR) Equation (1), including all terms except the second on the right-hand side. We analyze this problem for various geometries and boundary conditions.

2.2.1. Finite 1D Domain with Zero-Order Production: Dirichlet–Neumann Boundary Conditions

This section addresses the transient behaviour of contaminant transport with zero-order production in a finite one-dimensional domain. The problem is characterized by a Dirichlet boundary condition at one end, specifying the concentration, and a Neumann boundary condition at the other, representing an impervious boundary (see Figure 4). The boundary value problem of this scenario is given by

$$\begin{aligned} & \tfrac{1}{\alpha}\tfrac{\partial c}{\partial t} - \tfrac{\partial^2 c}{\partial x^2} + \tfrac{v}{D}\tfrac{\partial c}{\partial x} + \tfrac{\dot{m}}{D} = 0,\ \ 0 \le x \le L \\ & \text{IC}: \quad c\,(x,0) = 0 \\ & \text{BC}: \quad c\,(0,t) = C_0(t) \\ & \qquad \tfrac{\partial c}{\partial x}\Big|_{x=L} = 0 \end{aligned} \tag{24}$$

where $\alpha = D/R$ and $\dot{m}$ can be a function of ftime.

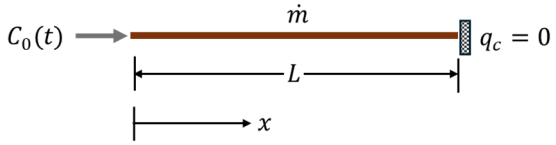

Figure 4. Finite domain with-order production: Dirichlet–Neumann.

Applying the Fourier transform to this BVP gives

$$\begin{gathered} \frac{i\omega}{\alpha}\hat{c} - \frac{d^2\hat{c}}{dx^2} + \frac{v}{D}\frac{d\hat{c}}{dx} + \frac{\dot{m}}{D} = 0 \\ \text{BC}: \ \hat{c}\,(0,\omega) = \hat{C}_0(\omega) \\ \left.\frac{d\hat{c}}{dx}\right|_{x=L} = 0 \end{gathered} \tag{25}$$

This boundary value problem is nonhomogeneous and can be solved via partitioning it into a homogeneous solution and a particular solution, such that

$$\hat{c} = \hat{c}_h + \hat{c}_p \tag{26}$$

The relevant homogenous part of the ODE in Equation (25) is

$$\frac{i\omega}{\alpha}\hat{c}_h - \frac{d^2\hat{c}_h}{dx^2} + \frac{v}{D}\frac{d\hat{c}_h}{dx} = 0 \tag{27}$$

As the coefficients are constant, the trial solution can be expressed as $\hat{c}_h = ae^{\kappa x}$. Substituting this trial solution into Equation (27) and solving the resulting algebraic equation, the general solution becomes

$$\begin{gathered} \hat{c}_h = a_1 e^{\kappa_1 x} + a_2 e^{\kappa_2 x} \\ \text{with} \\ \kappa_1 = \frac{\alpha v - \sqrt{\alpha^2 v^2 + 4i\alpha\omega D^2}}{2\alpha D}, \ \kappa_2 = \frac{\alpha v + \sqrt{\alpha^2 v^2 + 4i\alpha\omega D^2}}{2\alpha D} \end{gathered} \tag{28}$$

The relevant particular part of the ODE in Equation (25) is

$$\frac{i\omega}{\alpha}\hat{c}_p - \frac{d^2\hat{c}_p}{dx^2} + \frac{v}{D}\frac{d\hat{c}_p}{dx} + \frac{\dot{m}}{D} = 0 \tag{29}$$

As the nonhomogeneous (reaction) term is constant, the trial solution can be any constant, say $\hat{c}_p = A$. Substituting this trial solution into (29) and solving gives

$$\hat{c}_p = -\frac{\dot{m}\alpha}{i\omega D} \tag{30}$$

Substituting the homogeneous solution, Equation (28), and the particular solution, Equation (30), into Equation (26) yields the general solution of the differential equation in Equation (25), in the form

$$\hat{c} = a_1 e^{\kappa_1 x} + a_2 e^{\kappa_2 x} - \frac{\dot{m}\alpha}{i\omega D} \tag{31}$$

Applying the boundary conditions at $x = 0$, and $x = L$, and solving the resulting two equations simultaneously, the solution of the boundary value problem, Equation (25), in the frequency domain will then leads to

$$\hat{c}\,(x,\omega_n) = \frac{\hat{C}_0 + \frac{\dot{m}\alpha}{i\omega D}}{1 - \frac{\kappa_1}{\kappa_2}e^{(\kappa_1-\kappa_2)L}}e^{\kappa_1 x} + \frac{\hat{C}_0 + \frac{\dot{m}\alpha}{i\omega D}}{1 - \frac{\kappa_2}{\kappa_1}e^{(\kappa_2-\kappa_1)L}}e^{\kappa_2 x} - \frac{\dot{m}\alpha}{i\omega_n D} \tag{32}$$

Having solved the problem in the frequency domain, the contaminant distribution in the time domain can then be obtained using the inverse fast Fourier transform (IFFT) algorithm, such that

$$c\,(x,t)\;=\;\sum_n \hat{c}\,(x,\omega_n)\,e^{i\omega_n t} \tag{33}$$

Special case: Semi-infinite domain

As $L \to \infty$, the second term on the right-hand side of Equation (32) becomes unbounded and can be eliminated. Also, the denominator of the first term becomes 1, leading the solution to be

$$\hat{c}\,(x,\omega_n) = (\hat{C}_0 + \frac{\dot{m}\alpha}{i\omega D})\,e^{\kappa_1 x} - \frac{\dot{m}\alpha}{i\omega_n D} \tag{34}$$

2.2.2. Finite 1D Domain with Zero-Order Production: Robin–Neumann Boundary Conditions

This section considers the transient boundary value problem for contaminant transport with zero-order production in a finite one-dimensional domain. The domain is subjected to a Robin boundary condition at one end, modelling partial flux or interaction with the boundary, and a Neumann boundary condition at the other, representing an impervious boundary, as sketched in Figure 5. The problem is described by

$$\begin{aligned} &\tfrac{1}{\alpha}\tfrac{\partial c}{\partial t} - \tfrac{\partial^2 c}{\partial x^2} + \tfrac{v}{D}\tfrac{\partial c}{\partial x} + \tfrac{\dot{m}}{D} = 0, \qquad 0 \le x \le L \\ &\text{IC}: \quad c\,(x,0) = 0 \\ &\text{BC}: \quad -D\tfrac{\partial c}{\partial x}\Big|_{x=0} = v\,[\,C_0 - c\,(0,t)\,] \\ &\qquad\quad \tfrac{\partial c}{\partial x}\Big|_{x=L} = 0 \end{aligned} \tag{35}$$

in which C_0 (kgm^{-3}) is a contamination source at $x = 0$.

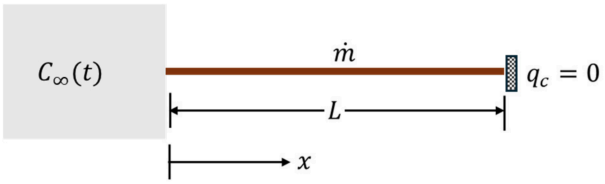

Figure 5. Finite domain with zero-order production: Robin–Neumann.

Applying the Fourier transform to this BVP gives

$$\begin{aligned} &\tfrac{i\omega}{\alpha}\hat{c} - \tfrac{d^2\hat{c}}{dx^2} + \tfrac{v}{D}\tfrac{d\hat{c}}{dx} + \tfrac{\dot{m}}{D} = 0 \\ &\text{BC}: \quad -D\tfrac{d\hat{c}}{dx}\Big|_{x=0} = v\,[\,\hat{C}_0 - \hat{c}(0,\omega)\,] \\ &\qquad\quad \tfrac{d\hat{c}}{dx}\Big|_{x=L} = 0 \end{aligned} \tag{36}$$

As discussed in the previous case, the general solution of this problem leads to

$$\begin{aligned} &\hat{c} = a_1 e^{\kappa_1 x} + a_2 e^{\kappa_2 x} - \tfrac{\dot{m}\alpha}{i\omega D} \\ &\text{with} \\ &\kappa_1 = \tfrac{\alpha v - \sqrt{\alpha^2 v^2 + 4i\alpha\omega D^2}}{2\alpha D},\ \kappa_2 = \tfrac{\alpha v + \sqrt{\alpha^2 v^2 + 4i\alpha\omega D^2}}{2\alpha D} \end{aligned} \tag{37}$$

Applying the boundary conditions at $x = 0$, and $x = L$, gives the complete solution of the boundary value problem in Equation (36), such that

$$\hat{c}\left(x, \omega_n\right) = \frac{v\left(\hat{C}_0 + \frac{\dot{m}\alpha}{i\omega D}\right)}{(v - D\kappa_1) - (v - D\kappa_2)\frac{\kappa_1}{\kappa_2} e^{(\kappa_1 - \kappa_2)L}} e^{\kappa_1 x} + \frac{-v\left(\hat{C}_0 + \frac{\dot{m}\alpha}{i\omega D}\right)}{(v - D\kappa_1)\frac{\kappa_2}{\kappa_1} e^{(\kappa_2 - \kappa_1)L} - (v - D\kappa_2)} e^{\kappa_2 x} - \frac{\dot{m}\alpha}{i\omega_n D} \tag{38}$$

in which

$$\alpha = \frac{D}{R}$$
$$\kappa_1 = \frac{\alpha v - \sqrt{\alpha^2 v^2 + 4i\alpha\omega D^2}}{2\alpha D},\ \kappa_2 = \frac{\alpha v + \sqrt{\alpha^2 v^2 + 4i\alpha\omega D^2}}{2\alpha D}$$

Having solved the problem in the frequency domain, the contaminant distribution in the time domain can then be obtained using the inverse fast Fourier transform (IFFT) algorithm, such that

$$c\left(x, t\right) = \sum_n \hat{c}\left(x, \omega_n\right) e^{i\omega_n t} \tag{39}$$

2.3. Contaminant Transport with Zero-Order Production and First-Order Decay

This scenario describes the transport of a chemical species undergoing simultaneous production and decay processes. The production occurs at a constant, concentration-independent rate (zero-order), while the decay follows first-order kinetics, with a rate proportional to the concentration.

The process is governed by the advection–dispersion–reaction (ADR) Equation (1), which incorporates the effects of advection, dispersion, and reaction. This framework enables the analysis of how production and decay interact to influence the contaminant's distribution and fate in various environmental settings. In this section, we solve the ADR equation for different geometries and boundary conditions, starting with the steady-state condition due to its practical significance.

2.3.1. Steady-State Contaminant Transport in a Finite 1D Domain with Dirichlet-Neumann Boundary Conditions

The steady-state boundary value problem governing advection–dispersion–reaction (ADR) contaminant transport in a finite one-dimensional domain subjected to a Dirichlet boundary condition at one end and a Neumann boundary condition (representing an impervious boundary) at the other (see Figure 6), is given by

$$\frac{d^2c}{dx^2} - \frac{v}{D}\frac{dc}{dx} - \frac{\mu}{D}c + \frac{\dot{m}}{D} = 0,\ 0 \le x \le L$$
$$\text{BC}: \ c\left(0\right) = C_0$$
$$\left.\frac{dc}{dx}\right|_{x=L} = 0 \tag{40}$$

where μ (s^{-1}) is some first-order decay coefficient.

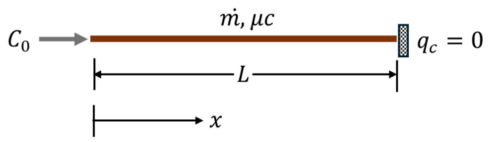

Figure 6. Dirichlet–Neumann steady state condition with production and decay.

The differential equation in Equation (40) is nonhomogeneous due to the presence of the reaction term $\dot{m}$. Following the solution procedure described earlier, we obtain

$$\begin{aligned} &c = a_1 e^{\kappa_1 x} + a_2 e^{\kappa_2 x} + \frac{\dot{m}}{\mu} \\ &\text{with} \\ &\kappa_1 = \frac{v}{2D} + \sqrt{\frac{\mu}{D} + \left(\frac{v}{2D}\right)^2},\ \kappa_2 = \frac{v}{2D} - \sqrt{\frac{\mu}{D} + \left(\frac{v}{2D}\right)^2} \end{aligned} \tag{41}$$

Applying the boundary conditions at $x = 0$ and $x = L$, the solution of this boundary value problem yields

$$c(x) = \frac{e^{\kappa_2 x} - e^{\kappa_1 x}}{\kappa_1 e^{\kappa_1 L} - \kappa_2 e^{\kappa_2 L}} \left(C_0 - \frac{\dot{m}}{\mu}\right) \kappa_2 e^{\kappa_2 L} + \left(C_0 - \frac{\dot{m}}{\mu}\right) e^{\kappa_2 x} + \frac{\dot{m}}{\mu} \tag{42}$$

Special case: Semi-infinite domain

As $L \to \infty$, the domain becomes semi-infinite. Since κ_1 is always positive, terms involving its exponent become unbounded, and hence the solution of this limiting case reduces to

$$\begin{aligned} &c(x) = \left(C_0 - \tfrac{\dot{m}}{\mu}\right) e^{\kappa_2 x} + \tfrac{\dot{m}}{\mu} \\ &\text{with} \\ &\kappa_2 = \tfrac{v}{2D} - \sqrt{\tfrac{\mu}{D} + \left(\tfrac{v}{2D}\right)^2} \end{aligned} \tag{43}$$

2.3.2. Finite 1D Domain with Robin–Neumann Boundary Conditions

The boundary value problem describing transient advection–dispersion–reaction (ADR) contaminant transport, exhibiting production and decay, in a finite 1D domain with a Robin boundary condition on one side and a Neumann boundary condition, representing a non-pervious domain, on the other side, (see Figure 7) is given by

$$\frac{1}{\alpha}\frac{\partial c}{\partial t} - \frac{\partial^2 c}{\partial x^2} + \frac{v}{D}\frac{\partial c}{\partial x} + \frac{\mu}{D}c - \frac{\dot{m}}{D} = 0,\ \ 0 \le x \le L$$

$$\begin{aligned} &\text{IC}: \quad c(x,0) = 0 \\ &\text{BC}: \quad -D\left.\frac{\partial c}{\partial x}\right|_{x=0} = v\left[C_0 - c(0,t)\right] \\ &\qquad\quad \left.\frac{\partial c}{\partial x}\right|_{x=L} = 0 \end{aligned} \tag{44}$$

with $\alpha = D/R$ and C_0 a contamination source. $\dot{m}$ and μ can be function of time.

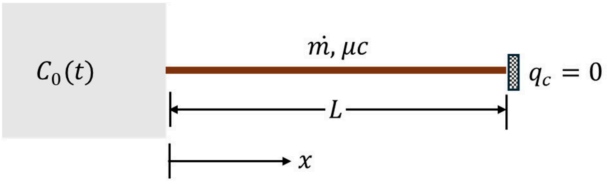

Figure 7. Robin–Neumann with production and decay.

Applying the Fourier transform to Equation (44) gives

$$\frac{i\omega}{\alpha}\hat{c} - \frac{d^2\hat{c}}{dx^2} + \frac{v}{D}\frac{d\hat{c}}{dx} + \frac{\mu}{D}\hat{c} - \frac{\dot{m}}{D} = 0$$

$$\begin{aligned} &\text{BC}: \quad -D\left.\frac{d\hat{c}}{dx}\right|_{x=0} = v\left[\hat{C}_0 - \hat{c}(0,\omega)\right] \\ &\qquad\quad \left.\frac{d\hat{c}}{dx}\right|_{x=L} = 0 \end{aligned} \tag{45}$$

This is a nonhomogeneous problem, and the solution requires solving both the homogeneous equation and the particular equation, such that

$$\hat{c} = \hat{c}_h + \hat{c}_p \tag{46}$$

Solving the corresponding homogenous differential equation of (45) and its associated particular solution results in

$$\begin{aligned} &\hat{c}\,(\omega) = a_1 e^{\kappa_1 x} + a_2 e^{\kappa_2 x} + \frac{\dot{m}}{D\,(\frac{i\omega}{\alpha} + \frac{\mu}{D})} \\ &\text{with} \\ &\kappa_1 = \frac{v}{2D} + \sqrt{\frac{\mu}{D} + (\frac{v}{2D})^2 + \frac{i\omega}{\alpha}},\ \kappa_2 = \frac{v}{2D} - \sqrt{\frac{\mu}{D} + (\frac{v}{2D})^2 + \frac{i\omega}{\alpha}} \end{aligned} \tag{47}$$

Applying the boundary conditions at $x = 0$ and $x = L$, solving the resulting two equations simultaneously, the solution in the frequency domain becomes

$$\begin{aligned} \hat{c}\,(x, \omega_n) = {} & \frac{\kappa_2 v}{\Delta}\left[\,\hat{C}_0 - \frac{\dot{m}}{D\,(\frac{i\omega_n}{\alpha} + \frac{\mu}{D})}\,\right] e^{\kappa_2 L} e^{\kappa_1 x} - \\ & \frac{\kappa_1 v}{\Delta}\left[\,\hat{C}_0 - \frac{\dot{m}}{D\,(\frac{i\omega_n}{\alpha} + \frac{\mu}{D})}\,\right] e^{\kappa_1 L} e^{\kappa_2 x} + \frac{\dot{m}}{D\,(\frac{i\omega_n}{\alpha} + \frac{\mu}{D})} \end{aligned} \tag{48}$$

where

$$\begin{aligned} &\Delta = (v - D\kappa_1)\,\kappa_2 e^{\kappa_2 L} - (v - D\kappa_2)\,\kappa_1 e^{\kappa_1 L} \\ &\alpha = \frac{D}{R} \\ &\kappa_1 = \frac{v}{2D} + \sqrt{\frac{\mu}{D} + (\frac{v}{2D})^2 + \frac{i\omega_n}{\alpha}},\ \kappa_2 = \frac{v}{2D} - \sqrt{\frac{\mu}{D} + (\frac{v}{2D})^2 + \frac{i\omega_n}{\alpha}} \end{aligned} \tag{49}$$

Having solved the problem in the frequency domain, the contaminant distribution in the time domain can then be calculated using the inverse fast Fourier transform (IFFT) algorithm, such that

$$c\,(x, t) = \sum_n \hat{c}\,(x, \omega_n)\, e^{i\omega_n t} \tag{50}$$

Special case 1: Semi-infinite domain

At the limiting case where $L \to \infty$, the domain becomes semi-infinite, and the solution in the frequency domain results in

$$\hat{c}\,(x, \omega_n) = \frac{v}{v - D\kappa_2}\left[\,\hat{C}_0 - \frac{\dot{m}}{D\,(\frac{i\omega_n}{\alpha} + \frac{\mu}{D})}\,\right] e^{\kappa_2 x} + \frac{\dot{m}}{D\,(\frac{i\omega_n}{\alpha} + \frac{\mu}{D})} \tag{51}$$

Special case 2: Steady state

As $\omega \to 0$, i.e., $t \to \infty$, the system reaches a steady state, and the solution becomes

$$\begin{aligned} &c\,(x) = \frac{v}{v - D\kappa_2}(\hat{C}_0 - \frac{\dot{m}}{\mu})\, e^{\kappa_2 x} + \frac{\dot{m}}{\mu} \\ &\text{with} \\ &\kappa_2 = \frac{v}{2D} - \sqrt{\frac{\mu}{D} + (\frac{v}{2D})^2} \end{aligned} \tag{52}$$

Example 1. *Effect of production/decay processes and distribution coefficient.*

In this example, we investigate how production and decay processes affect the spatial distribution of a chemical species within a porous medium and assess the impact of the distribution coefficient, which governs adsorption, on this behavior. The domain under consideration is a fully saturated porous medium, 150 m in length, with a bulk density of 1600 kg/m^3 and a porosity of 0.3. One boundary of the domain is exposed

to a chemical species characterized by a distribution coefficient of 0.001 m^3/kg and a hydrodynamic dispersion coefficient of 1.5 m^2/d. Groundwater flows through the domain at an average velocity of 0.5 m/d. Figure 8 schematically shows the geometry and boundary conditions. Initially, the domain contains no concentration of the chemical species. At the inlet boundary ($x = 0$), a Robin-type boundary condition is applied, featuring a bell-shaped concentration profile as illustrated in Figure 9. The outlet boundary ($x = L$) is sealed by an impervious layer, preventing any further transport of the species.

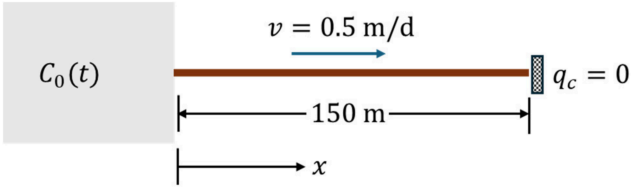

Figure 8. Geometry and boundary conditions.

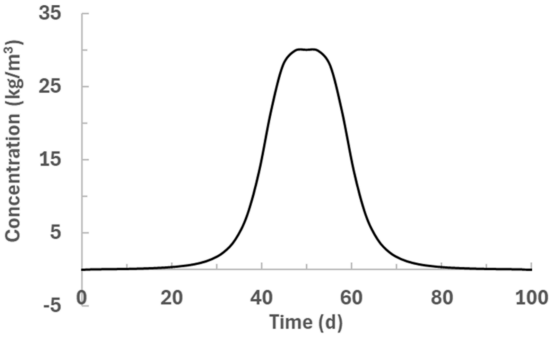

Figure 9. Species concentration around $x = 0$.

Under certain conditions, the species might be exposed to a zero-order production of 0.1 kg/md and/or first-order decay of 0.001 d^{-1}, The time distribution of these two factors follow the same time profile as that of the source, see Figure 9. We examine four scenarios:

1. No production and no decay.
2. With production but without decay.
3. With decay but without production.
4. With production and decay.

We also examine two possible distribution coefficients: 0.01 and 0.001 d^{-1}.

To solve this problem, the time domain was discretized into 2^{13} (8192) FFT samples with a sampling interval of 0.1 day.

The computational results depicting species distribution over time at various spatial locations along the domain for the four scenarios are presented in Figure 10. The figure highlights the dynamic interplay between production rate and the effect of decay over time and space. As expected, scenarios involving production exhibit higher concentrations compared to those without, while scenarios incorporating decay show reduced concentrations. The influence of production and decay becomes more pronounced at greater distances from the source. Figure 11 displays the species concentration for the four scenarios at a location 10 m from the source. It is evident that increased production leads to higher species concentrations within the domain, which also persist for longer durations.

Figure 12 illustrates the influence of the sorption, represented by the distribution coefficient K_d, on the spatial concentration of the species within the domain. The results indicate that higher values of K_d lead to enhanced partitioning between phases, thereby promoting greater dispersion of the species. This suggests a direct correlation between sorption and the extent of species spread, reflecting its critical role in governing transport dynamics.

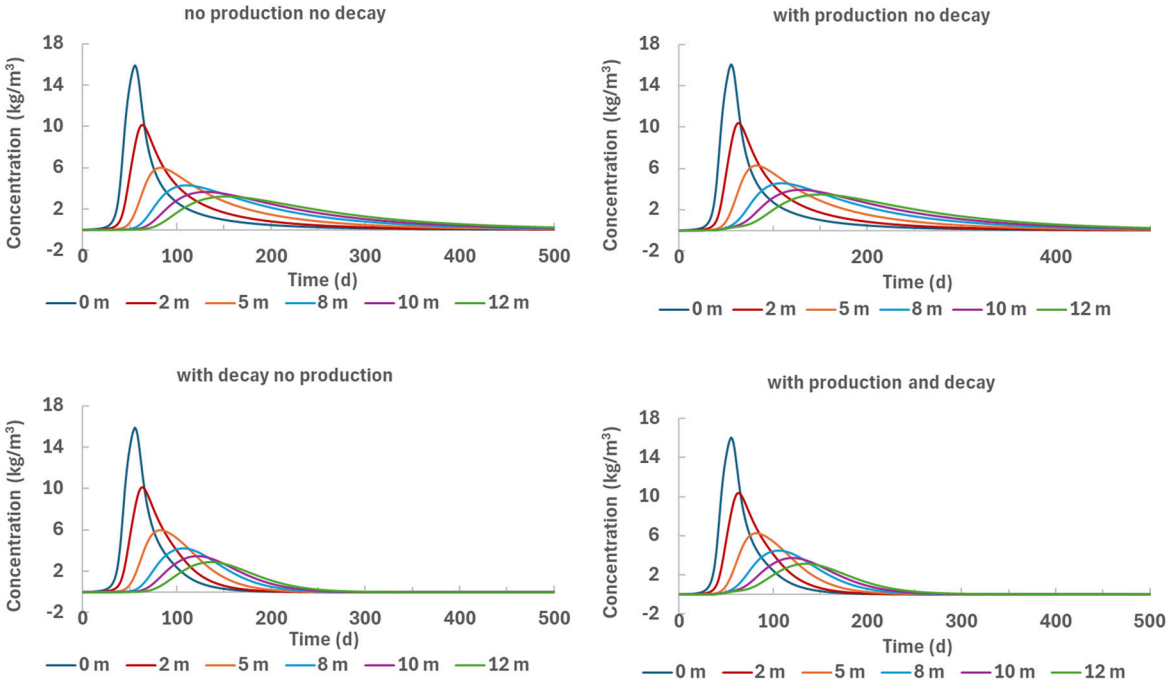

Figure 10. Pollutant time variation at different spatial locations.

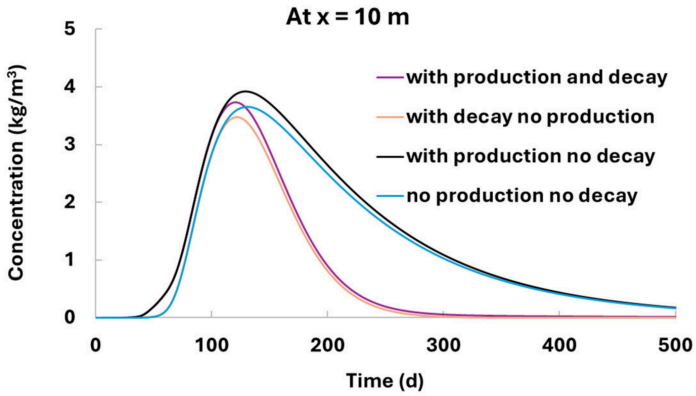

Figure 11. Behavior of the pollutant under the four scenarios.

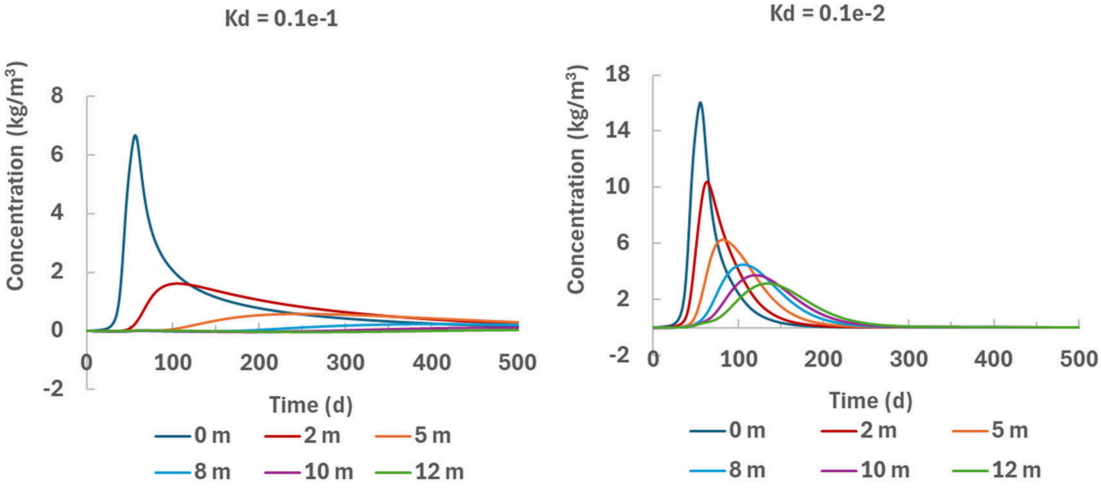

Figure 12. Influence of sorption (K_d) on the species concentration.

2.4. Model Verification

In this section, the Fourier-FFT model for first-order decay and zero-order production is evaluated against the analytical solution given by van Genuchten and Alvis [13] using the Laplace transform approach. The objective is twofold: first, to demonstrate the accuracy of the proposed model; and second, to emphasize the relative simplicity and computational convenience of the Fourier-FFT approach compared with the Laplace transform method.

The governing boundary value problem addressed by van Genuchten and Alvis [13] is given by

$$\begin{aligned} R\frac{\partial c}{\partial t} &= D\frac{\partial^2 c}{\partial x^2} - v\frac{\partial c}{\partial x} - \mu c + \gamma \\ c\,(x,0) &= c_i \\ \left(-D\frac{\partial c}{\partial x} + vc\right)\Big|_{x=0} &= \begin{cases} vC_0 & 0 < t < t_0 \\ 0 & t > t_0 \end{cases} \\ \frac{\partial c}{\partial x}\Big|_{x=L} &= 0 \end{aligned} \tag{53}$$

where γ represents the production rate, resembling $\dot{m}$ in our formulation.

Using the Laplace transform, they proposed two ways to solve the problem: analytical and approximate.

Analytical solution

$$c\,(x,t) = \begin{cases} \frac{\gamma}{\mu} + (c_i - \frac{\gamma}{\mu})A\,(x,t) + (C_0 - \frac{\gamma}{\mu})B\,(x,t) & 0 < t < t_0 \\ \frac{\gamma}{\mu} + (c_i - \frac{\gamma}{\mu})A\,(x,t) + (C_0 - \frac{\gamma}{\mu})B\,(x,t) - C_0 B\,(x,t-t_0) & t > t_0 \end{cases} \tag{54}$$

where

$$\begin{aligned} A\,(x,t) &= \sum_{m=1}^{\infty} E(\beta_m, x)\exp\left[\frac{vx}{2D} - \frac{\mu t}{R} - \frac{v^2 t}{4DR} - \frac{\beta_m^2 Dt}{L^2 R}\right] \\ B\,(x,t) &= B_1(x) - B_2(x,t) \end{aligned} \tag{55}$$

with

$$\begin{aligned} B_1(x) &= 1 - \frac{\mu L^2}{D}\sum_{m=1}^{\infty} \frac{E(\beta_m, x)\exp\left(\frac{vx}{2D}\right)}{\left[\beta_m^2 + \left(\frac{vL}{2D}\right)^2 + \frac{\mu L^2}{D}\right]} \\ B_2(x,t) &= \sum_{m=1}^{\infty} \frac{E(\beta_m, x)\left[\beta_m^2 + \left(\frac{vL}{2D}\right)^2\right]\exp\left[\frac{vx}{2D} - \frac{\mu t}{R} - \frac{v^2 t}{4DR} - \frac{\beta_m^2 Dt}{L^2 R}\right]}{\beta_m^2 + \left(\frac{vL}{2D}\right)^2 + \frac{\mu L^2}{D}} \end{aligned} \tag{56}$$

and

$$E(\beta_m, x) = \frac{\frac{2vL}{D}\beta_m\left[\beta_m\cos\left(\frac{\beta_m x}{L}\right) + \frac{vL}{2D}\sin\left(\frac{\beta_m x}{L}\right)\right]}{\left[\beta_m^2 + \left(\frac{vL}{2D}\right)^2 + \frac{vL}{D}\right]\left[\beta_m^2 + \left(\frac{vL}{2D}\right)^2\right]} \tag{57}$$

The eigenvalues β_m are the positive roots of

$$\beta_m\cot(\beta_m) - \frac{\beta_m^2 D}{vL} + \frac{vL}{4D} = 0 \tag{58}$$

Van Genuchten and Alves stated that the term $B_1(x)$ converges much slower than the other terms, and provided an alternative form that is easier to evaluate, given by

$$B_1(x) = \frac{\exp\left[\frac{(v-u)\,x}{2D}\right] + \left(\frac{u-v}{u+v}\right)\exp\left[\frac{(v+u)\,x-2uL}{2D}\right]}{\frac{u+v}{2v} - \frac{(u-v)^2}{2v\,(u+v)}\exp\left(-\frac{uL}{D}\right)} \tag{59}$$

with

$$u = v\sqrt{1+\frac{4\mu D}{v^2}} \tag{60}$$

Approximate solution

According to van Genuchten and Alves, the Analytical solution converges slowly for relatively large values of the Peclet number, $P = vL/D$. For relatively large Peclet number problems, they provided an approximate solution, given hereafter.

$$\begin{aligned} A\,(x,t) = \exp\left(-\mu t/R\right)\Big\{1 - \tfrac{1}{2}\mathrm{erfc}\left[\tfrac{Rx-vt}{2(DRt)^{1/2}}\right] - \\ \left(\tfrac{v^2 t}{\pi DR}\right)^{1/2}\exp\left[-\tfrac{(Rx-vt)^2}{4DRt}\right] + \\ \tfrac{1}{2}\left[1+\tfrac{vx}{D}+\tfrac{v^2 t}{DR}\right]\exp\left(vx/D\right)\mathrm{erfc}\left[\tfrac{Rx+vt}{2(DRt)^{1/2}}\right] - \\ \left(\tfrac{4v^2 t}{\pi DR}\right)^{1/2}\left[1+\tfrac{v}{4D}(2L-x+\tfrac{vt}{R})\right]\exp\left[\tfrac{vL}{D}-\tfrac{R}{4Dt}(2L-x+\tfrac{vt}{R})^2\right] + \\ \tfrac{v}{D}\left[2L-x+\tfrac{3vt}{2R}+\tfrac{v}{4D}(2L-x+\tfrac{vt}{R})^2\right]\exp\left(vL/D\right)\,\mathrm{erfc}\left[\tfrac{R(2L-x)+vt}{2(DRt)^{1/2}}\right]\Big\} \end{aligned} \tag{61}$$

$$B(x,t) = B_3(x,t)/B_4(x)$$

where

$$\begin{aligned} B_3(x,t) = \tfrac{v}{(v+u)}\exp\left[\tfrac{(v-u)\,x}{2D}\right]\mathrm{erfc}\left[\tfrac{Rx-ut}{2(DRt)^{1/2}}\right] + \\ \tfrac{v}{(v-u)}\exp\left[\tfrac{(v+u)\,x}{2D}\right]\mathrm{erfc}\left[\tfrac{Rx+ut}{2(DRt)^{1/2}}\right] + \\ \tfrac{v^2}{2\mu D}\exp\left(\tfrac{vx}{D}-\tfrac{\mu t}{R}\right)\mathrm{erfc}\left[\tfrac{Rx+vt}{2(DRt)^{1/2}}\right] + \\ \tfrac{v^2}{2\mu D}\left[\tfrac{v(2L-x)}{D}+\tfrac{v^2 t}{DR}+3+\tfrac{v^2}{\mu D}\right]\exp\left(\tfrac{vL}{D}-\tfrac{\mu t}{R}\right)\mathrm{erfc}\left[\tfrac{R(2L-x)+vt}{2(DRt)^{1/2}}\right] - \\ \tfrac{v^3}{\mu D}\left(\tfrac{t}{\pi DR}\right)^{1/2}\exp\left[\tfrac{vL}{D}-\tfrac{\mu t}{R}-\tfrac{R}{4Dt}(2L-x+\tfrac{vt}{R})^2\right] + \\ \tfrac{v\,(u-v)}{(u+v)^2}\exp\left[\tfrac{(v+u)x-2uL}{2D}\right]\mathrm{erfc}\left[\tfrac{R(2L-x)-ut}{2(DRt)^{1/2}}\right] - \\ \tfrac{v\,(u+v)}{(u-v)^2}\exp\left[\tfrac{(v-u)x+2uL}{2D}\right]\mathrm{erfc}\left[\tfrac{R(2L-x)+ut}{2(DRt)^{1/2}}\right] \end{aligned} \tag{62}$$

$$B_4(x) = 1 - \tfrac{(u-v)^2}{(u+v)^2}\exp\left(-uL/D\right)$$

According to van Genuchten and Alves, this approximate solution is accurate if it meets any of these two conditions:

$$\frac{vL}{D} > 5 + 40\frac{vt}{RL}, \text{ or } \frac{vL}{D} > 100 \tag{63}$$

A verification case

We present a verification case comparing the proposed Fourier model with the van Genuchten model for solving the advection–dispersion–reaction (ADR) equation governing contaminant transport in a finite one-dimensional domain. A geometry and physical configuration similar to that adopted in Example 1 of Section 2.3.2 is employed here, with minor adjustments to ensure compatibility with the van Genuchten and Alves solution.

Figure 8 schematically shows the geometry and boundary conditions of the domain. Initially, the concentration of the chemical species is zero throughout. At the inlet boundary ($x = 0$), a Robin boundary condition is applied, characterized by a block-shaped concentration profile, as illustrated in Figure 13. The outlet boundary ($x = L$) is sealed by an impervious layer, preventing any further transport of the species. The physical parameters are as follows:

- Length (L): 150 m
- Bulk density (ρ): 1600 kg/m^3
- Porosity (φ): 0.3
- Distribution coefficient (K_d): 0.001 m^3/kg
- Hydrodynamic dispersion coefficient (D): 1.5 m^2/d
- Groundwater flows velocity (v): 0.5 m/d
- Production ($\dot{m}$, (γ in van Genuchten)): 0.1 kg/md
- Decay coefficient (μ): -0.001 d^{-1} (Note that the negative value of the decay coefficient μ used here is due to the different sign convention adopted in the governing equation of van Genuchten and Alves, Equation (53), relative to the formulation used in the present study, Equation (44).)

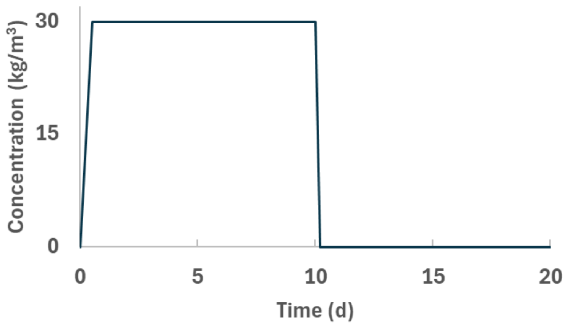

Figure 13. Input boundary pulse.

The time distribution of $\dot{m}$ (γ) and μ follows a similar time profile as that of the source (see Figure 13), though they extend over twice the time span.

Two scenarios have been examined:

1. No production and no decay.
2. With production and decay.

Solution

We implemented both van Genuchten's solutions (Analytical and Approximate) using the mathematical software, MAPLE 2024.2 [28]. To find the eigenvalues of Equation (58), we employed Halley's method (also known as the cubic convergence root-finding method or refined Newton's method) for root-finding. Despite considerable attempts, the Analytical solution failed to converge. Consequently, we adopted the Approximate solution for verification. For solving this problem using the Fourier-FFT approach, the time domain was discretized into 2^{13} (8192) FFT samples with a sampling interval of 0.1 day.

Figure 14 shows the comparison between the two models, for both scenarios: without decay or production, and with both included. The figure clearly demonstrates a perfect match for the case without decay or production, and a reasonably good match for the other scenario. The slight mismatch between the two solutions may be attributed either to the approximation inherent in the van Genuchten model or to the assumption of a time-independent production term (γ). In the van Genuchten formulation, production begins instantaneously at every spatial point in the domain, even before the arrival of the species, and continues throughout the entire analysis period.

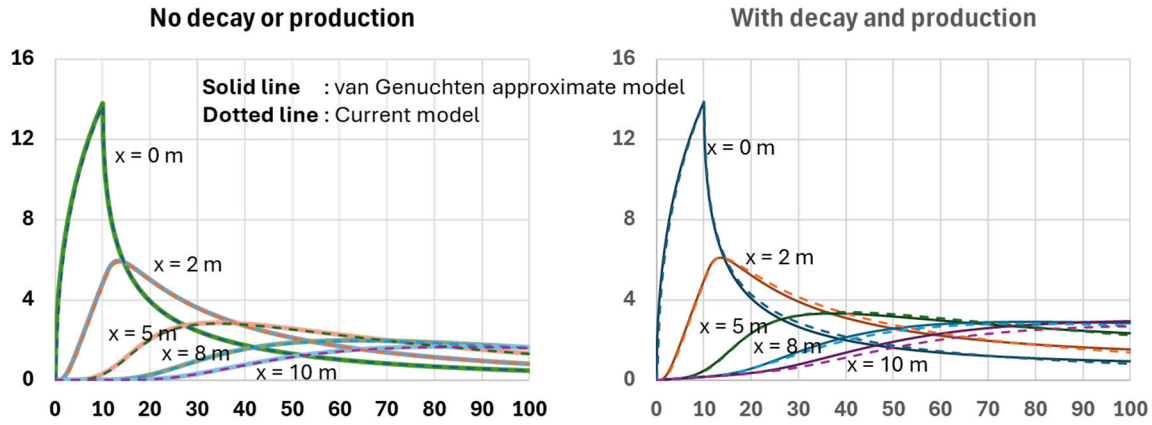

Figure 14. Comparison between current, proposed model and van Genuchten Approximate model.

3. One-Dimensional Contaminant Transport in Dual Permeability Domains

The dual permeability method, also referred to as the double permeability method, is a conceptual framework in environmental engineering and hydrogeology used to model fluid flow and contaminant transport in heterogeneous porous media. Unlike the traditional single permeability or equivalent porous medium approach, this method distinguishes between two separate flow domains within the porous medium: the solid matrix and the fracture network. The solid matrix typically consists of finer, low-permeability material, while the fracture network comprises interconnected, high-permeability pathways. By explicitly accounting for this dual structure, the method offers a more precise depiction of complex contaminant transport processes, making it an important tool for understanding and addressing groundwater pollution.

The boundary value problem for a contaminant transport in a double permeability semi-infinite domain undergoing first-order decay with no production on both components and exposed to a Dirichlet boundary condition, can be expressed as

$$\begin{aligned} R_m \frac{\partial c_m}{\partial t} + v_m \frac{\partial c_m}{\partial x} - D_m \frac{\partial^2 c_m}{\partial x^2} &= -\alpha \left(c_m - c_f\right) - \mu_m c_m \\ R_f \frac{\partial c_f}{\partial t} + v_f \frac{\partial c_f}{\partial x} - D_f \frac{\partial^2 c_f}{\partial x^2} &= \alpha \left(c_m - c_f\right) - \mu_f c_f \end{aligned}$$

$$\begin{aligned} \text{IC}: \quad & c_m(x,0) = c_f(x,0) = 0 \\ \text{BC}: \quad & c_m(0,t) = C_{m0}(t) \\ & c_f(0,t) = C_{f0}(t) \\ & c_m(\infty,t) = c_f(\infty,t) = 0 \end{aligned} \tag{64}$$

where the subscripts m and f refer to the species concentration in the matrix and fracture components, respectively, and α is a transfer coefficient between the two domains. The physical parameters in Equation (64) are defined in Section 2.

Transforming Equation (64) into the frequency domain gives

$$\begin{aligned} D_m \frac{d^2 \hat{c}_m}{dx^2} - v_m \frac{d\hat{c}_m}{dx} - \left(i\omega R_m + \alpha + \mu_m\right) \hat{c}_m + \alpha \hat{c}_f &= 0 \\ D_f \frac{d^2 \hat{c}_f}{dx^2} - v_f \frac{d\hat{c}_f}{dx} - \left(i\omega R_f + \alpha + \mu_f\right) \hat{c}_f + \alpha \hat{c}_m &= 0 \end{aligned}$$

$$\begin{aligned} \text{BC}: \hat{c}_m(0,\omega) &= \hat{C}_{m0}(\omega) \\ \hat{c}_f(0,\omega) &= \hat{C}_{f0}(\omega) \\ \hat{c}_m(\infty,\omega) &= \hat{c}_f(\infty,\omega) = 0 \end{aligned} \tag{65}$$

As the coefficients of the differential equations in Equation (65) are constant, the trial solutions can be

$$\begin{aligned} \hat{c}_m &= A\, e^{-\kappa x} \\ \hat{c}_f &= B\, e^{-\kappa x} \end{aligned} \tag{66}$$

where A, B and κ are constants to be determined. Substituting these solutions into the differential equations in Equation (65), and rearranging, yields

$$\begin{aligned} D_m\kappa^2 A + v_m\kappa A - (i\omega R_m + \alpha + \mu_m)\, A + \alpha B = 0 \\ D_f\kappa^2 B + v_f\kappa B - (i\omega R_f + \alpha + \mu_f)\, B + \alpha A = 0 \end{aligned} \tag{67}$$

Incorporating these two equations in a matrix format gives

$$\begin{pmatrix} G_m & \alpha \\ \alpha & G_f \end{pmatrix} \begin{pmatrix} A \\ B \end{pmatrix} = \begin{pmatrix} 0 \\ 0 \end{pmatrix} \tag{68}$$

with

$$\begin{aligned} G_m &= D_m\kappa^2 + v_m\kappa - (i\omega R_m + \alpha + \mu_m) \\ G_f &= D_f\kappa^2 + v_f\kappa - (i\omega R_f + \alpha + \mu_f) \end{aligned} \tag{69}$$

The solution of Equation (68) can only be attained if we set the determinate of the matrix to zero. This results in a fourth order polynomial equation of the form

$$m_4\kappa^4 + m_3\kappa^3 + m_2\kappa^2 + + m_1\kappa + m_0 = 0 \tag{70}$$

where κ represents the four eigenvalues of the system. Following this, the general solutions of both mediums become

$$\begin{aligned} \hat{c}_m &= A_1 e^{-\kappa_1 x} + A_2 e^{-\kappa_2 x} + A_3 e^{-\kappa_3 x} + A_4 e^{-\kappa_4 x} \\ \hat{c}_f &= B_1 e^{-\kappa_1 x} + B_2 e^{-\kappa_2 x} + B_3 e^{-\kappa_3 x} + B_4 e^{-\kappa_4 x} \end{aligned} \tag{71}$$

The third boundary conditions in Equation (65) implies that the coefficients associated with the positive exponential terms in Equation (71) are irrelevant since they result in an unbounded solution at far distances. This implies

$$\begin{aligned} \hat{c}_m &= A_1 e^{-\kappa_1 x} + A_2 e^{-\kappa_2 x} \\ \hat{c}_f &= B_1 e^{-\kappa_1 x} + B_2 e^{-\kappa_2 x} \end{aligned} \tag{72}$$

As the two species are coupled, their constants must be related, expressed via the eigenvectors of the system. The constants A and B in Equation (68) are related via

$$\begin{aligned} &B_j = Y_i A_j \\ &\text{with} \\ &Y_j = -\tfrac{G_m}{\alpha} \end{aligned} \tag{73}$$

with j denoting that for each eigenvalue κ_j there is a corresponding eigenvector. Following this, Equation (72) can be expressed as

$$\begin{aligned} \hat{c}_m &= A_1 e^{-\kappa_1 x} + A_2 e^{-\kappa_2 x} \\ \hat{c}_f &= Y_1 A_1 e^{-\kappa_1 x} + Y_2 A_2 e^{-\kappa_2 x} \end{aligned} \tag{74}$$

At $x = 0$, the first and second boundary conditions in Equation (65) imply

$$\begin{aligned} A_1 + A_2 &= \hat{C}_{0m} \\ Y_1 A_1 + Y_2 A_2 &= \hat{C}_{0f} \end{aligned} \tag{75}$$

Solving these two equations simultaneously leads to

$$\begin{aligned} A_1 &= \frac{\hat{C}_{0f} - Y_2\hat{C}_{0m}}{Y_1 - Y_2} \\ A_2 &= \hat{C}_{0m} - A_1 \end{aligned} \tag{76}$$

Substituting Equation (76) into Equation (74), the solution of the BVP in Equation (65) for a given frequency ω_n can be expressed as

$$\begin{aligned} \hat{c}_m(x,\omega_n) &= \frac{\hat{C}_{0f} - Y_2\hat{C}_{0m}}{Y_1 - Y_2}(e^{-\kappa_1 x} - e^{-\kappa_2 x}) + \hat{C}_{0m}e^{-\kappa_2 x} \\ \hat{c}_f(x,\omega_n) &= \frac{\hat{C}_{0f} - Y_2\hat{C}_{0m}}{Y_1 - Y_2}(Y_1 e^{-\kappa_1 x} - Y_2 e^{-\kappa_2 x}) + Y_2\hat{C}_{0m}e^{-\kappa_2 x} \end{aligned} \tag{77}$$

with

$$Y_j = -\frac{1}{\alpha}[D_m\kappa_j^2 + v_m\kappa_j - (i\omega R_m + \alpha + \mu_m)] \tag{78}$$

Following this, the solution in the time domain can then be obtained via the inverse FFT algorithm, such that

$$\begin{aligned} c_m(x,t) &= \textstyle\sum_n \hat{c}_m(x,\omega_n)\, e^{i\omega_n t} \\ c_f(x,t) &= \textstyle\sum_n \hat{c}_f(x,\omega_n)\, e^{i\omega_n t} \end{aligned} \tag{79}$$

Model Verification and Parametric Analysis

In this section, the Fourier-FFT solution of the dual-permeability system is verified against numerical results obtained using the finite-element software COMSOL Multiphysics 6.4 [29]. Solute transport in COMSOL is simulated with the Transport of Diluted Species in Porous Media (TDS-PM) interface.

Using both approaches, we study the influence of the decay coefficient μ and sorption, represented by the distribution coefficient K_d, on contaminant transport in a dual-permeability system. By varying these parameters, we assess their contributions to plume attenuation and to mass exchange between the matrix and fracture domains. We consider contaminant transport in a 1D dual-permeability domain with the following model parameters:

- Diffusion/dispersion: $D_m = D_f = 1.5\ \mathrm{m^2/d}$
- Sorption and material properties: $f = 0.4$, $b = 0.01\ 1/\mathrm{d}$, $\rho_{\mathrm{bulk}} = 1800.0\ \mathrm{kg/m^3}$, with $K_d = 0.0$ and $K_d = 0.001\ (\mathrm{m^3 kg^{-1}})$.
- Decay coefficients: $\mu_m = \mu_f = 0$ and $\mu_m = \mu_f = 0.1\ 1/\mathrm{d}$.
- Porosities: $\phi_m = 0.3$, $\phi_f = 0.3$.
- Velocities: $v_m = 0.5\ \mathrm{m/d}$, $v_f = 2.0\ \mathrm{m/d}$.

The domain is subjected to a Dirichlet boundary condition at $x = 0$, with a maximum concentration of $10\ \mathrm{kg/m^3}$ and a time-dependent input profile, as shown in Figure 15. To solve this problem using the Fourier-FFT approach, the time domain was discretized into 2^{14} (16,384) FFT samples with a sampling interval of 0.005 day.

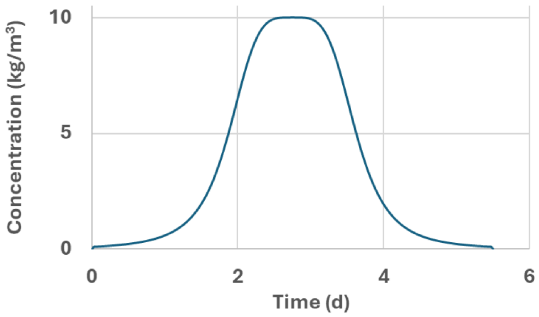

Figure 15. Input concentration.

COMSOL evaluates the governing equations of the TDS-PM interface strictly using moles and seconds as base units. For analyses without sorption, i.e., $K_d = 0$, no modification of the concentration input is required, aside from converting time-dependent parameters from days to seconds. However, when sorption is included, the inlet boundary condition must be adjusted to account for the unit conversion between mass- and molar-based concentrations, such that

$$c_{\text{Comsol}}(\text{mol/m}^3) = \frac{c_{\text{Fourier-FFT}}(\text{kg/m}^3)}{M}$$

where M is the molar mass (kg/mol). Comparing the computational results therefore requires multiplying the COMSOL-predicted concentrations by the molar mass to recover mass-based concentrations consistent with the analytical formulation. Accordingly, COMSOL results are post-processed as $M\,c_{\text{Comsol}}$ to enable direct comparison with the Fourier-FFT solution.

The temporal concentration distribution for the case with zero K_d and no decay ($\mu_m = \mu_f = 0$) is presented in Figure 16. The figure demonstrates good match between the two solution approaches. Physically, the results indicate that concentrations remain consistently higher within the fracture domain, reflecting its rapid transport relative to the matrix.

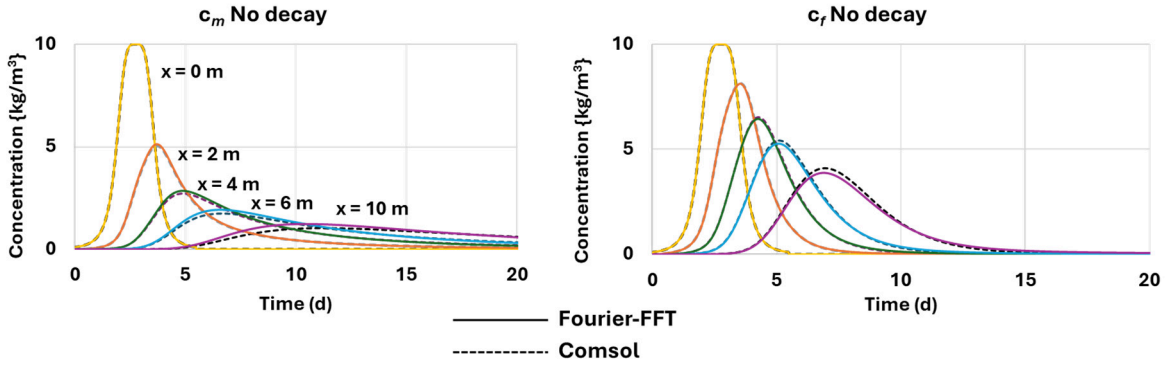

Figure 16. Concentration distribution for the case with no sorption and no decay.

Figure 17 shows a rather good agreement between the Fourier-FFT solution and COMSOL computational results for the case with decay but no sorption.

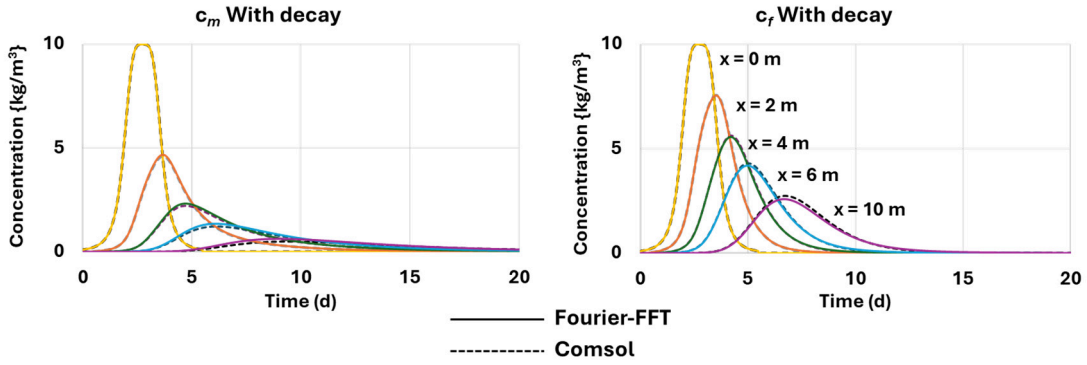

Figure 17. Concentration distribution for the case with decay but no sorption.

Figure 18 demonstrates the matching between the two approaches for the case with sorption ($K_d = 0.001$ m^{3}kg^{-1}) and decay ($\mu_m = \mu_f = 0.1$ d^{-1}). Again, the two solutions agree well with each other.

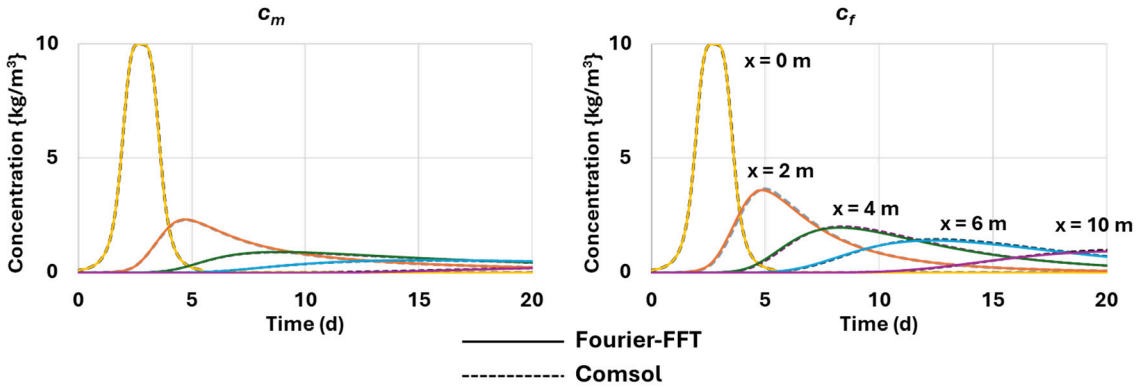

Figure 18. Concentration distribution for the case with sorption and decay.

Figure 19 illustrates the influence of sorption on contaminant transport by comparing two simulations with different values of the distribution coefficient: $K_d = 0.0$ and $K_d = 0.001$ (m^3kg^{-1}). As expected, increasing K_d leads to stronger retardation of the solute, resulting in lower concentrations and noticeably delayed breakthrough in both domains, with the effect being particularly pronounced in the fracture network. The contrast between the two cases clearly highlights the role of sorption in moderating plume migration and reducing mass transfer into the fracture network.

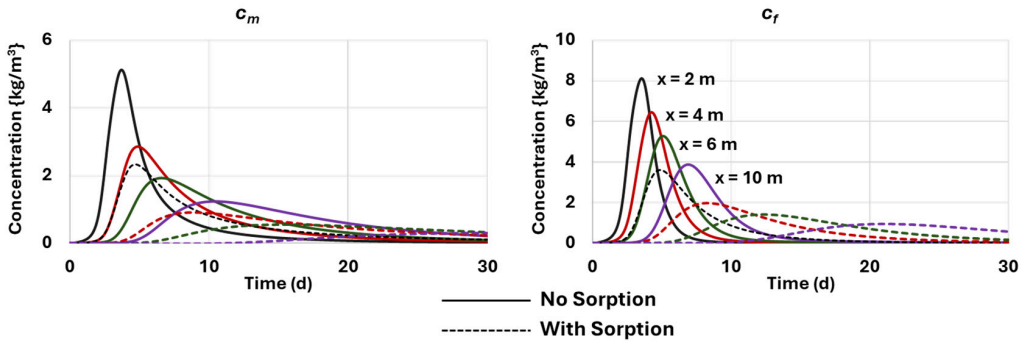

Figure 19. Influence of sorption on contaminant transport.

Figure 20 illustrates the impact of decay on contaminant transport by comparing two simulations with different decay rates: $\mu_m = \mu_f = 0$ and $\mu_m = \mu_f = 0.1$ d^{-1}. Increasing the decay rate leads to a reduction in concentrations and a delay in breakthrough across both domains, with the attenuation effect being particularly pronounced within the fracture network. This influence becomes increasingly evident at greater distances from the source, where the cumulative impact of decay results in more substantial plume attenuation.

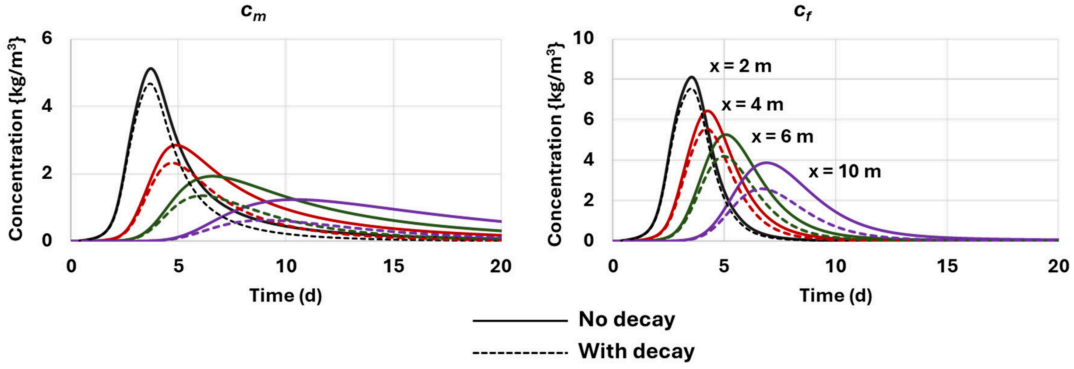

Figure 20. Impact of decay on contaminant transport.

4. Conclusions

This paper establishes an analytical framework for modelling contaminant transport in homogeneous and heterogeneous one-dimensional porous media. The study demonstrates that the use of the Fourier method, enhanced by the fast Fourier transform (FFT), provides an elegant and systematic methodology for solving boundary value problems of varying complexity.

While the Laplace transform is a powerful analytical tool for the forward transform of partial differential equations, its inverse often results in complex semi-infinite integrals involving convolution of transcendental functions. The derivation of the advection–dispersion (AD) equation presented by Ogata and Banks [20] illustrates the mathematical complexity inherent in Laplace inversion, even for simple transport problems, highlighting the difficulty of deriving such solutions without considerable mathematical expertise. In contrast, the inverse FFT is straightforward, fast, and readily available in most mathematical software, making the overall Fourier-FFT framework both accessible and computationally efficient. A comparison between the solution procedure presented in Section 2.1 and that of Ogata and Banks clearly demonstrates the fundamental differences between the two approaches, emphasizing the simplicity and practicality of the Fourier-FFT framework.

Moreover, unlike Laplace-transform approaches, which are limited to idealized inputs such as pulses or step functions, the fast Fourier transform inherently accommodates realistic, arbitrarily time-varying boundary conditions, making the proposed modelling approach particularly suitable for real-world scenarios where contaminant inputs rarely follow simple or instantaneous patterns.

This paper illustrates the versatility of the proposed Fourier-FFT framework in modelling both homogeneous and heterogeneous porous media systems, including coupled dual-permeability domains characterized by distinct fracture and matrix transport behaviours. From a physical perspective, the dual-permeability formulation captures coupled transport within two hydraulically active continua, where both fractures and the porous matrix maintain advective flow at different velocities. The results show that preferential transport through fractures occurs simultaneously with slower migration in the matrix, while inter-domain mass exchange controls concentration redistribution, plume attenuation, and breakthrough behaviour. The parametric analyses further show that sorption enhances solute retardation and reduces fracture mobility, whereas decay progressively attenuates contaminant concentrations during transport. These findings emphasize the importance of explicitly representing fracture–matrix interactions when predicting contaminant migration, breakthrough timing, and long-term plume persistence in heterogeneous subsurface environments.

Therefore, by employing the Fourier-FFT solution technique to the advection–dispersion–reaction equation, this work illustrates how realistic analytical models can be systematically formulated and implemented without extensive mathematical training. This straightforward approach enables engineers and applied scientists to tailor and solve boundary value problems for their specific needs, facilitating advanced calculations in practical applications and enhancing understanding of contaminant transport in subsurface environments.

Author Contributions: Conceptualization, R.a.K.; methodology, R.a.K.; software, C.K.; validation, C.K. and R.a.K.; formal analysis, R.a.K. and C.K.; investigation, R.a.K. and C.K.; writing—original draft preparation, R.a.K.; writing—review and editing, R.a.K. and C.K.; visualization, C.K. and R.a.K. All authors have read and agreed to the published version of the manuscript.

Funding: This research received no external funding.

Data Availability Statement: No new data were created.

Conflicts of Interest: The authors declare no conflict of interest.

References

1. Fetter, C.W. *Contaminant Hydrogeology*, 2nd ed.; Prentice Hall: Hoboken, NJ, USA, 1999.
2. Yeh, G.T. *Computational Subsurface Hydrology: Reactions, Transport, and Fate*; Springer: Berlin/Heidelberg, Germany, 2000.
3. Zheng, C.; Bennett, G.D. *Applied Contaminant Transport Modeling*; Wiley: Hoboken, NJ, USA, 2002.
4. Selim, H.M. *Transport & Fate of Chemicals in Soils: Principles & Applications*; CRC Press: Boca Raton, FL, USA, 2015.
5. Goltz, M.; Huang, J. *Analytical Modeling of Solute Transport in Groundwater*; Wiley: Hoboken, NJ, USA, 2017.
6. Idelsohn, S.; Nigro, N.; Storti, M.; Buscaglia, G.A. A Petrov-Galerkin formulation for advection-reaction-diffusion problems. *Comput. Methods Appl. Mech. Eng.* **1996**, *136*, 27–46. [CrossRef]
7. Sheu, T.W.H.; Chen, Y.H. Finite element analysis of contaminant transport in groundwater. *Appl. Math. Comput.* **2002**, *127*, 23–43. [CrossRef]
8. Javadi, A.A.; Al-Najjar, M.M. Finite element modeling of contaminant transport in soils including the effect of chemical reactions. *J. Hazard. Mater.* **2007**, *143*, 690–701. [CrossRef] [PubMed]
9. Leij, F.J.; Toride, N.; van Genuchten, M.T. Analytical solutions for non-equilibrium solute transport in three-dimensional porous media. *J. Hydrol.* **1993**, *151*, 193–228. [CrossRef]
10. Leij, F.J.; Priesack, E.; Schaap, M.G. Solute transport modeled with Green's functions with application to persistent solute sources. *J. Contam. Hydrol.* **2000**, *41*, 155–173. [CrossRef]
11. Clement, T.P. Generalized solution to multispecies transport equations coupled with a first-order reaction network. *Water Resour. Res.* **2001**, *37*, 157–163. [CrossRef]
12. Sangani, J.; Srivastava, A.; Srinivasan, V. Analytical solutions to three-dimensional reactive contaminant transport problems involving point, line, and area sources. *Transp. Porous Media* **2022**, *144*, 641–667. [CrossRef]
13. van Genuchten, M.T.; Alves, W.J. *Analytical Solutions of the One-Dimensional Convective-Dispersive Solute Transport Equation*; U.S. Department of Agriculture: Washington, DC, USA, 1982.
14. van Genuchten, M.T. Analytical solutions for chemical transport with simultaneous adsorption, zero-order production, and first-order decay. *J. Hydrol.* **1981**, *49*, 213–233. [CrossRef]
15. van Genuchten, M.T. Convective-dispersive transport of solutes involved in sequential first-order decay reactions. *Comput. Geosci.* **1985**, *11*, 129–147. [CrossRef]
16. Leij, F.J.; Dane, J.H.; van Genuchten, M.T. Mathematical analysis of one-dimensional solute transport in a layered soil profile. *Soil Sci. Soc. Am. J.* **1991**, *55*, 944–953. [CrossRef]
17. van Genuchten, M.T.; Leij, F.J.; Todd, S.; Toride, N.; Bradford, S.A.; Ponteiro, E.M. Exact analytical solutions for contaminant transport in rivers. 1. The equilibrium advection-dispersion equation. *J. Hydrol. Hydromech.* **2013**, *61*, 146–160. [CrossRef]
18. van Genuchten, M.T.; Leij, F.J.; Todd, S.; Toride, N.; Bradford, S.A.; Ponteiro, E.M. Transient storage and decay chain solutions. *J. Hydrol. Hydromech.* **2013**, *61*, 250–259.
19. Park, E.; Zhan, H. One-dimensional solute transport in a permeable reactive barrier aquifer system. *Water Resour. Res.* **2009**, *45*, W07502. [CrossRef]
20. Ogata, A.; Banks, R.B. A solution of the differential equation of longitudinal dispersion in porous media. In *U.S. Geological Survey Professional Paper 411-A*; United States Department of the Interior, Geological Survey: Reston, VA, USA, 1961.
21. Sousa, E. Fourier transform methods for fractional advection-diffusion equations. *Proc. Appl. Math. Mech.* **2012**, *12*, 699–700.
22. Hasanov, A.; Erturk, V.S.; Gupta, P.K. Spectral collocation solutions for fractional advection-dispersion equations. *Appl. Math. Comput.* **2015**, *266*, 1–14.
23. Zhan, W.; Zhuang, M.; Liu, Q.Q.; Shi, L.; Sun, Y.; Liu, Q.H. Frequency domain spectral element method for modelling poroelastic waves in 3-D anisotropic, heterogeneous and attenuative porous media. *Geophys. J. Int.* **2021**, *227*, 1339–1353. [CrossRef]
24. Luo, X.; Chen, X.H.; Li, T.; Luo, G.R.; Wang, P. Numerical analysis of dispersion, attenuation, and seismic effects in a porous rock saturated with three-phase immiscible fluids. *Pet. Sci.* **2025**, *22*, 2828–2850. [CrossRef]
25. Bai, Y.; Yang, T.; Liu, C. Analytical solutions of advection-dispersion equations in porous media using integral transform techniques. *Adv. Water Resour.* **2015**, *83*, 127–137.
26. Doyley, J.F. *Wave Propagation in Structures*, 3rd ed.; Springer: Berlin/Heidelberg, Germany, 2021.
27. Al Khoury, R.; Kasbergen, C. *Analytical Subsurface Environment: Heat Transfer, Groundwater Flow and Contaminant Transport*; Springer: Berlin/Heidelberg, Germany, 2026.
28. Maplesoft. *Maple 2024.2*; Maplesoft, a division of Waterloo Maple Inc.: Waterloo, ON, Canada, 2024.
29. COMSOL AB. *COMSOL Multiphysics® Version 6.4*; COMSOL AB: Stockholm, Sweden, 2024.